Miner Petrol (2012) 106:151–171
DOI 10.1007/s00710-012-0228-4

ORIGINAL PAPER

Thermodynamic modeling assisted by multivariate statistical image analysis as a tool for unraveling metamorphic *P-T-d* evolution: an example from *ilmenite-garnet-bearing* metapelite of the Peloritani Mountains, Southern Italy

Patrizia Fiannacca · Deborah Lo Pò · Gaetano Ortolano · Rosolino Cirrincione · Antonino Pezzino

Received: 29 November 2011 / Accepted: 8 October 2012 / Published online: 21 October 2012

Abstract An ilmenite-garnet-bearing schist from the medium-grade metapelite complex of the Mandanici Unit in the Peloritani Mountains has been investigated to constrain the P-T conditions attained in this sector of the southern European Hercynian chain. Microprobe investigations assisted by statistical handling of X-ray maps via principal component analysis allowed us to better elucidate the porphyroblast-matrix relationships, the geometry of the elemental distribution in garnet porphyroblasts and the average volume percentage of the reactant garnet during retrograde metamorphic evolution. Selected microprobe data were then used to constrain, by means of P-T pseudosections, the main P-T stages of the metamorphic evolution, using the XRF bulk-rock chemistry as the equilibrium chemical composition for the prograde and peak stages and an effective bulk-rock composition for the retrograde one. Peak metamorphic P-T estimates (~530 °C; 0.9 GPa) are consistent with a Hercynian crustal thickening stage at middle-lower crustal conditions, while subsequent evolution, constrained at 420–460 °C; 0.30–0.60 GPa, depicts a retrograde clockwise P-T trajectory linked to exhumation under likely extensional shearing conditions. The results obtained in this paper lead to envisage a new scenario for the crustal evolution of the Peloritani Mountains and stimulate a revision of previous interpretations in the light of the new investigation techniques.

Editorial handling: G. Hoinkes

P. Fiannacca · G. Ortolano (✉) · R. Cirrincione · A. Pezzino
Department of Biological, Geological and Environmental Sciences, University of Catania,
Corso Italia 57,
95129 Catania, Italy
e-mail: ortolano@unict.it

D. Lo Pò
Department of Earth and Geoenvironmental Sciences,
University of Bologna,
Piazza di Porta San Donato 1,
40126 Bologna, Italy

Introduction

Integrated microstructural and microprobe investigations are essential tools to obtain information about progressive foliation development, porphyroblast growth-timing and chemical zoning patterns, in turn necessary to constrain through geothermobarometry the different stages of pressure-temperature-deformation (P-T-d) evolution of metamorphic rocks.

Significant advances in P-T path reconstructions have been made with the development of the techniques of thermodynamic modeling of representative samples via computation of P-T pseudosections (e.g. Holland and Powell 1998; White et al. 2000; Connolly and Petrini 2002; Connolly 2005, 2009). Nevertheless, high reliability of achieved constraints may be ensured only if the thermodynamically derived data closely match the actual structural and minerochemical features of studied rocks, with particular reference to the correct sequence of mineral equilibria (e.g. Zeh 2001; Gaidies et al. 2006; Cirrincione et al. 2008; Angì et al. 2010; Groppo and Castelli 2010).

For this reason, the most detailed P-T paths have been usually obtained on medium-grade porphyroblastic metapelites, known to be particularly well suited to reconstruct reliable sequences of blasto-deformational events. Indeed, lack of porphyroblasts in lower grade metamorphics often prevents to obtain meaningful blasto-deformational relationships while, in high-grade rocks, both earlier foliations and

paragenetic equilibria are frequently completely obliterated and/or chemically re-homogenized by the latest pervasive metamorphic stages.

In this paper thermodynamic modeling of a medium-grade metapelite has been carried out by integrating thermobarometric, microstructural, mineral association and minerochemical data. Besides, in an attempt to minimize the risk of personal bias in the determination of reliable mineral equilibria, a new image processing technique developed by means of multivariate image statistical data handling via GIS based tools, has been applied to X-ray maps of representative micro-domains, to help identifying effective equilibrium assemblages and reaction volumes. Computation of P-T pseudosections before and after fractionation effects constrained by means of this technique proved to be very useful to quantify the composition and relative percentage of effective equilibrium assemblages.

In more detail, a sample of porphyroblastic ilmenite-garnet bearing schist cropping out locally in the Mandanici Unit of the Peloritani Mountains has been selected for the purpose of the present study. Indeed, no detailed P-T path has been up to now elaborated for the basement rocks of this segment of the original southern European Hercynian belt, likely also because of the absence of suitable parageneses in the low- and very-low-grade metamorphic rocks of the Peloritani Mountains (Cirrincione et al. 2012) and of the pervasive late-Hercynian thermal re-equilibration in the medium- to high-grade metamorphic rocks (Appel et al. 2011). In particular, the selected metapelite sample is characterized by i) well-preserved porphyroblast-matrix relationships, ii) fine grained matrix able to record a multistage deformational sequence and, iii) apparent absence of compositional porphyroblasts re-equilibration by diffusion processes.

This sample was studied integrating microstructural and microprobe investigations with thermodynamic modelling (Connolly and Petrini 2002; Cirrincione et al. 2008 and reference therein) assisted by image processing of X-ray maps, with the aim of reliably estimating the sequence of P-T conditions attained during its orogenic cycle. This approach proved to be extremely useful and provided precious novel information about the tectono-metamorphic evolution of a segment of the Hercynian belt exposed in the Peloritani Mountains.

Geological setting

Peloritani Mountains (NE Sicily) are the southernmost part of the Calabria-Peloritani Orogen (CPO), an Alpine nappe-pile edifice located between the NW-SE-trending Southern Apennine and EW-trending Siculo-Maghrebide chains (Fig. 1a). They constitute a very complex continental crust sector (Ferla 2000), structured in a collisional belt and subdivided into the Lower Complex, outcropping in the southern part of the Peloritani Mountains, and the Upper Complex, exposed in the northern part of the chain (Cirrincione et al. 1999, 2012) (Fig. 1b).

The Lower Complex comprises three tectonic units composed by very-low to low-grade Hercynian metamorphic rocks (below the chlorite-isograd, $T \leq 350$ °C, $P \geq 2$ Kb; Atzori and Ferla 1992) and sedimentary covers, both unaffected by Alpine metamorphic re-equilibration.

The Upper Complex comprises the most internal nappes of the Peloritani Mountains, and it is constituted by the low- to medium-grade Mandanici Unit (MU) and the overlying medium-high grade Aspromonte-Peloritani Unit (APU), which crops out also in the Aspromonte Massif (southern Calabria). The basement rocks of the latter unit are mainly composed of paragneisses and augen gneisses and minor micaschists, amphibolites and marbles, produced by a polyphase HT-LP retrograde Hercynian metamorphism (Pezzino et al. 1990; Puglisi and Pezzino 1994) and later intruded by late Hercynian granitoids (Fiannacca et al. 2008; and reference therein).

The MU consists of relatively low pressure, low to medium temperature rocks with paragenetic equilibria consistent with upper greenschist to lower amphibolite-facies conditions (Atzori and Sassi 1973). Very few, and mostly only qualitative, data are available about the P-T metamorphic conditions of the MU rocks. Atzori and Ferla (1992; and reference therein) describe the MU as a unit mainly composed of epizonal to mesozonal metamorphic rocks and report similar P-T clockwise evolution of the metamorphic rocks of MU and APU, with thermal and baric peaks achieved at $T < 620$ °C and $P < 5.5$ Kbar, respectively, for the highest grade rocks, as deduced from mineral assemblages and conventional geothermobarometry. Phyllites are the dominant MU lithotypes, while quarzites, marbles, metabasites and micaschists are subordinate (Cirrincione and Pezzino 1991; Ferla 2000). The metamorphic grade increases towards the present-day upper levels of the unit (Ferla 1972), suggesting an overturned setting, further confirmed by the presence of an anchimetamorphic Mesozoic sedimentary cover (i.e. Alì Series) at the bottom of the present-day structural framework, interpreted as the original cover of the crystalline basement involved in the Alpine metamorphic cycle (Cirrincione and Pezzino 1991; Cirrincione et al. 2012).

Although an Alpine subgreenschist- to greenschist-facies metamorphic overprint at relatively high pressure has been locally documented in the Mandanici and Aspromonte-Peloritani Units (Atzori et al. 1994; Pezzino et al. 2008 and references therein), the Hercynian orogeny has long been considered responsible for the main metamorphic events in the Peloritani Mountains (Atzori et al. 1994; De Gregorio et al. 2003; Appel et al. 2011). Dubois and Truillet (1971) suggested that the Mandanici Unit was the sedimentary cover of a pre-Hercynian basament metamorphosed during the Hercynian orogeny, whereas Ferla (2000; and

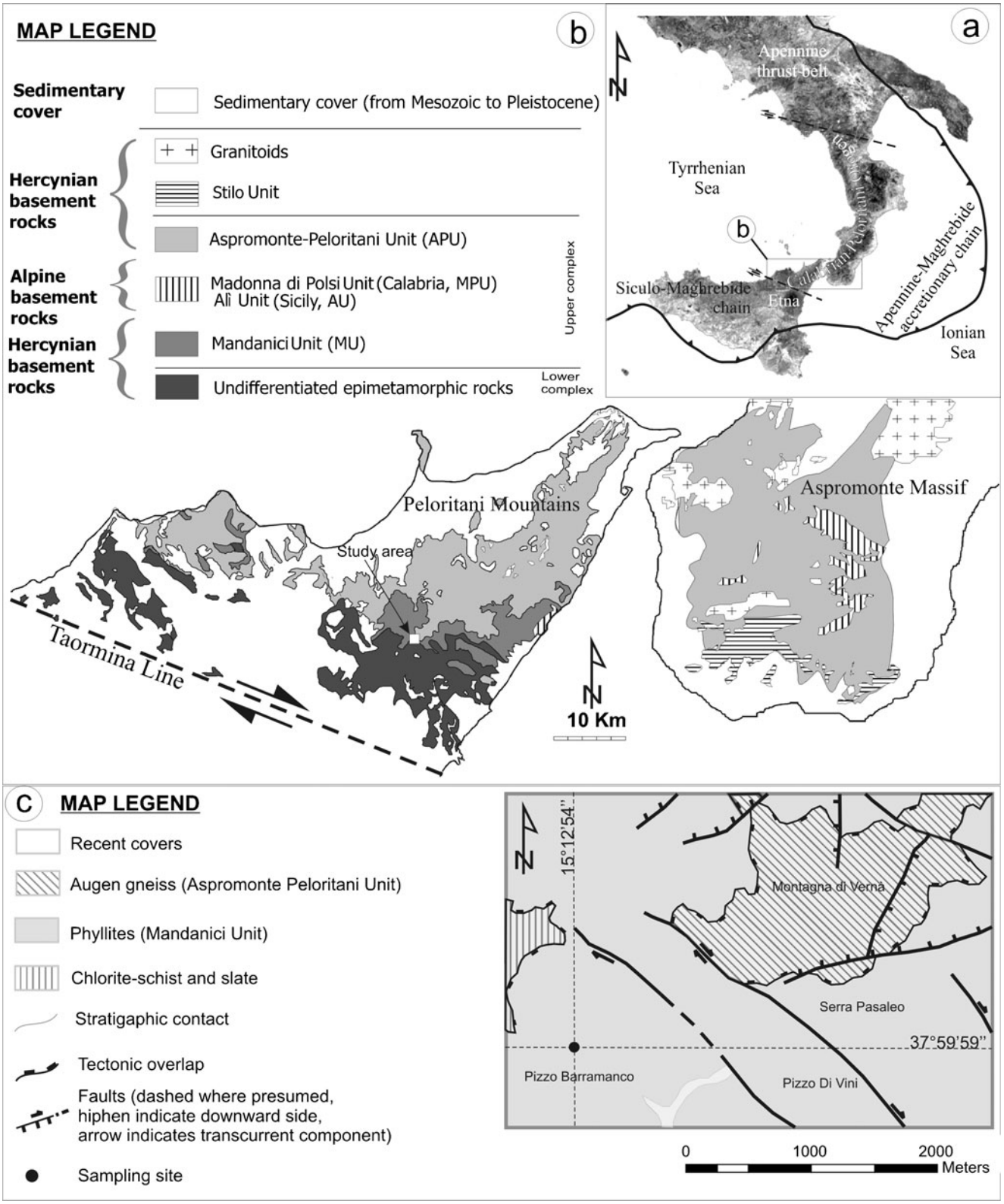

Fig. 1 Regional geological framework of the study area: **a**) Southern Italy with location of Calabrian Peloritani Orogen; **b**) Geological sketch map of the Peloritani Mountains and Aspromonte Massif crystalline basement complexes with the subdivision of the tectono-metamorphic units (from Cirrincione et al., 2012, modified); **c**) Geological sketch map of the study area with sample location (from Lentini et al., 2000, modified)

reference therein) proposed a pre-Hercynian origin of the whole Upper Complex basement. According to the latter author the basement of the Upper Complex would have been pervasively reworked by the Hercynian metamorphism together with its Paleozoic sedimentary cover, presently represented by the basement units of the Lower Complex. Recent SHRIMP U-Pb zircon studies carried out on paragneiss and augen gneiss samples of the Aspromonte-Peloritani Unit (Williams et al. 2012; Fiannacca et al., 2012) have demonstrated that large portions of the unit formed during the latest stages of the Avalonian-Cadomian orogeny (~550 Ma). As far as the Mandanici Unit is concerned, most authors still consider it as composed of Early Paleozoic volcano-sedimentary sequences turned into low-grade metamorphic rocks during the Hercynian orogeny (e.g., Russo et al. 2006; Ferla and Meli 2007).

Petrographic and microstructural features

Three thin sections of an ilmenite-garnet schist sample cropping out in the Vernà Mountain area (Fig. 1c) have been examined; one of them cut parallel and the other two perpendicular to the mesoscopic lineation, given by microfold axial culmination, in order to ensure identification of all the structural features produced by the succession of deformational stages, as well as to provide precise information on the 3D distribution of the fabric and on the modal abundances of the mineral constituents.

The selected schist is characterized by a dominant lepidoblastic microstructure (Fig. 2a), with poikilitic garnet and ilmenite porphyroblasts (Fig. 2b–d) wrapped by alternating muscovite+chlorite and minor quartz+plagioclase layers, with apatite, monazite and zircon as accessory phases. Three schistosity surfaces were recognized: S_1, recognizable only at the thin section scale, consists of an isoclinal folding schistosity, largely obliterated and only preserved as microfold hinge relics within the granoblastic domains between S_2 layers (Fig. 2a–e); the second one (S_2), which represents the main foliation to be observed in the field, is a penetrative and pervasive crenulation schistosity generated by a non-coaxial deformational event (D_2). It also produced rotated porphyroblasts (Fig. 2b); the last one (S_3), clearly recognizable only in the porphyroclast pressure shadows as well as between fragments of pinch-and-swell garnet porphyroclasts (Fig. 2f), was generated by a retrograde non-coaxial shearing event (D_3) also responsible for the formation of mica-fish.

Rock-forming minerals, in decreasing order of abundance (Fig. 3), are:

White mica (36.5 vol.%) characterized by three different crystallization stages. The first one is only recognizable by the presence of structural relics in the microfold hinges. The second generation comprises aggregates of small flakes parallel to the main schistosity S_2, while the third generation crystallizes in the pressure shadows of former porphyroblasts during D_3 shearing stage.

Quartz (35.6 vol.%) constitutes equidimensional blasts, with undulose extinction and S_2-parallel elongation. It is concentrated as granoblastic layers in the fold hinges, as large crystals around garnets in the pressure-shadows, and as σ-shaped inclusion trails in garnet cores.

Chlorite (20.1 vol.%) is localized along the S_1 relic surfaces, in the S_2 planes in association with white mica and in garnet pressure-shadows. Total to partial polycrystalline chlorite pseudomorphs after garnet are locally observed.

Plagioclase (4.8 vol.%) occurs both in the matrix and as minor porphyroblasts mostly elongated parallel to S_2.

Elongated, or roundish-shaped, poikiloblastic garnet (1.7 vol.%) exhibits quartz and rarer ilmenite inclusion trails, well preserved in garnet core, defining a σ-shaped internal schistosity (S_2) (Fig. 2b, c). This observation suggests that garnet crystallized during the second metamorphic event (M_2), incorporating quartz and ilmenite that produced an internal foliation continuous with the external schistosity represented by the S_2 surface (Fig. 2b). Syn-kinematic garnet was locally overgrown by unfolded rims, masking the original crenulated garnet morphology (Fig. 2c). The D_3 shearing event induced porphyroblast rotation, which evolved locally to the formation of mica-fish and stretched and pinch-and-swell garnet porphyroclasts suggesting extensional shearing conditions; growth of retrograde chlorite and muscovite occurred during this stage (Fig. 2f).

Ilmenite accounts for 1.4 vol.% in the sample: euhedral crystals are parallel to S_1 or mechanically re-oriented throughout S_2. It shows occasionally reaction rims and recurrent leucoxene alteration interpreted as retrograde reaction (e.g. Raase et al. 1986) (Fig. 2d).

Accessory minerals are represented by apatite, usually in association with monazite or included in garnet, monazite in foliation-aligned mostly anhedral grains, and zircon, mostly occurring as partly corroded grains.

Microstructural analysis permitted to reconstruct the metamorphic-deformational relationships, highlighting a polyphase deformation evolution. The attention was focused especially on garnet porphyroblastic domains useful for interpreting the sequence of the tectono-metamorphic stages. During M_1 the stable mineralogical assemblage, partly preserved in microlithons, comprised quartz, white mica I generation, ilmenite plus, probably, chlorite I and plagioclase I generations. The synkinematic mineral phases with respect to M_2, representing the dominant event recorded in the rock, are quartz, white mica II, chlorite II, plagioclase II, ilmenite reaction rims and rotated garnet porphyroblasts, overgrown by inclusion-free rims. Although M_3 was a dominantly mechanical event, blastesis of quartz, chlorite III, and white mica III can be locally observed.

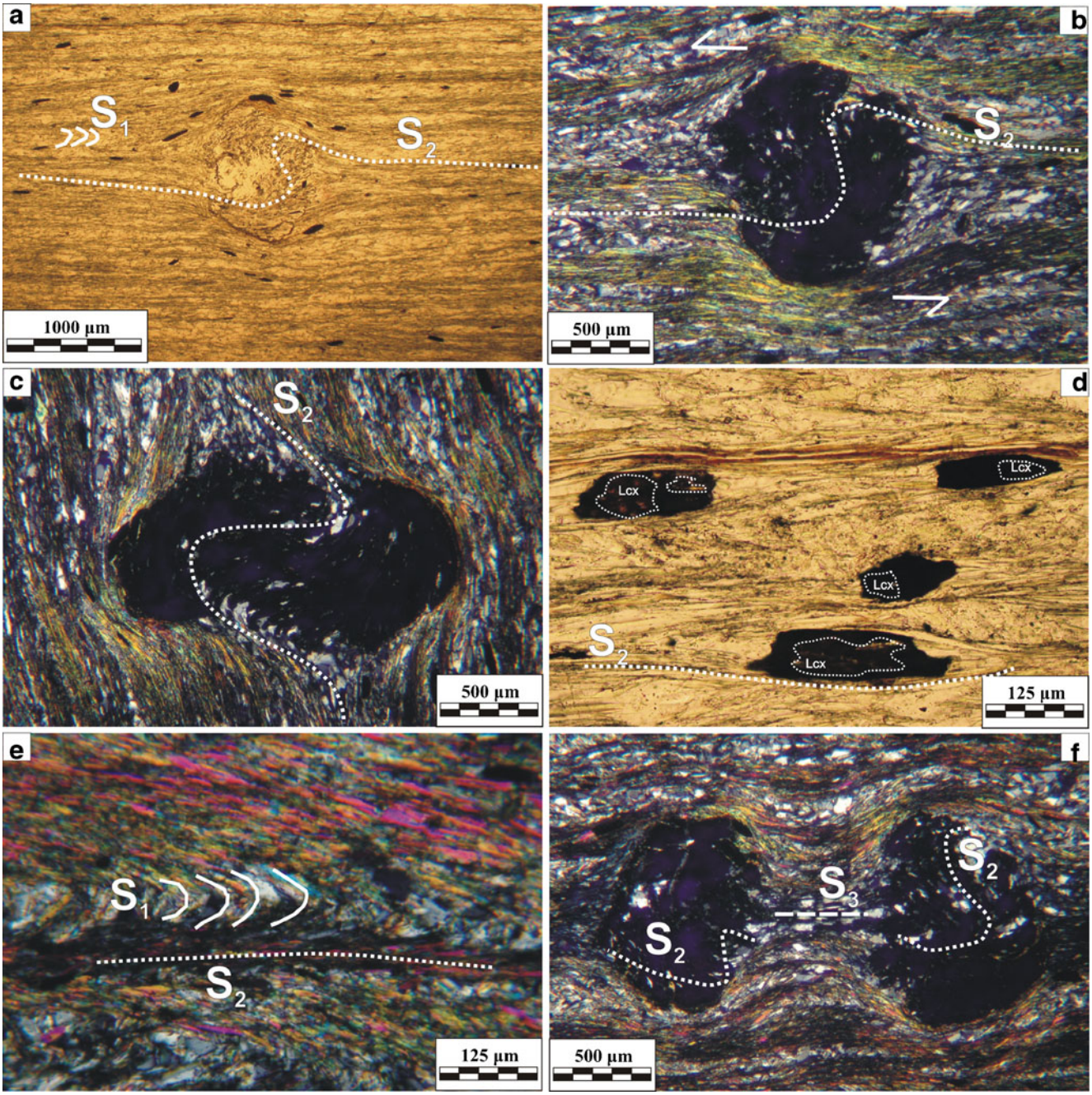

Fig. 2 Petrographical features: **a**) general microstructure given by a fine-grained matrix depicting a dominant lepidoblastic texture (*parallel polars*); **b**) poikiloblastic garnet with folded inclusion trails surrounded by dominant muscovite+chlorite lepidoblastic layers and subordinate quartz+plagioclase granoblastic layers (*crossed polars*); **c**) evidence of late- to post-kinematic garnet overgrowth (crossed polars); **d**) ilmenite porphyroblasts mechanically re-oriented along the crenulation schistosity (*parallel polars*); **e**) symmetric microfold hinge relics preserved within the granoblastic domains (*crossed polars*); **f**) pinch-and-swell garnet porphyroblasts (*crossed polars*)

Whole-rock chemistry

Whole-rock composition was obtained through XRF analysis on pressed powder pellets, performed on a Philips PW 2404 spectrometer equipped with a Rh anticathode at the Department of Biological, Geological and Environmental Sciences, Catania University, corrected for matrix effects (Franzini et al. 1972); FeO content was determined by titration with potassium permanganate, H_2O was measured as weight loss on ignition (L.O.I.) and was determined with standard gravimetric procedures, after heating the powder at ~900 °C for about 6 h. Whole-rock chemistry was used to derive information about the rock protolith, assuming a dominantly isochemical metamorphism and to obtain the

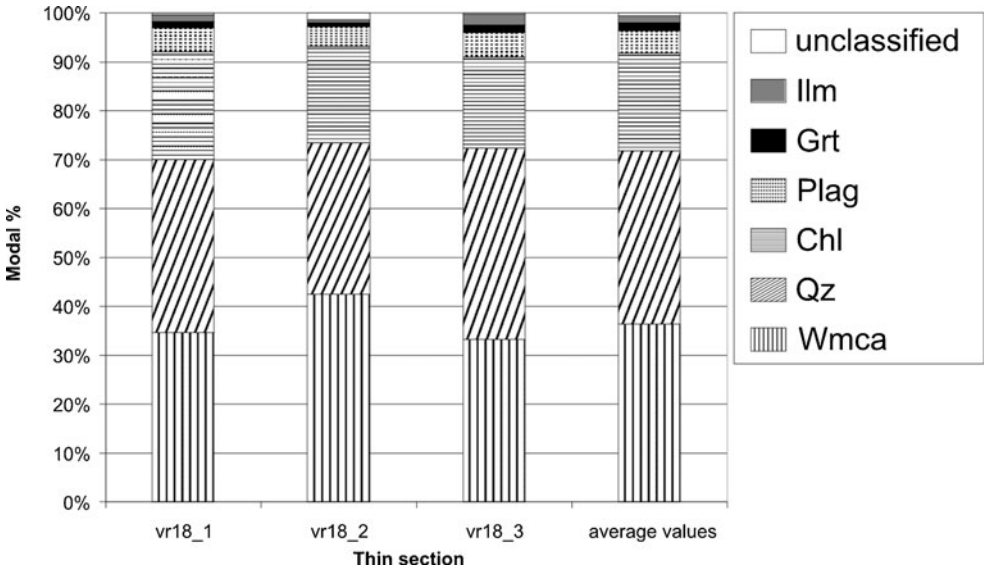

Fig. 3 Histogram of the point counting analysis (1,000 points per thin section)

chemical composition of the equilibrium volume useful to calculate P-T pseudosections.

The studied sample plots as shale in classification diagrams (e.g. De La Roche 1978; Herron 1988) and within the field representative of Mandanici Unit phyllites compositions. Normalization of the chemical composition to PAAS (Post-Archean Australian Shale; Taylor and McLennan 1985) also shows a composition similar to average shales, except for lower CaO contents (0.38 wt.% in the studied sample compared to 1.3 wt.% in PAAS), possibly because of a low concentration of $CaCO_3$, as sediment component or as authigenic product, in the original basin.

Mineral-chemistry and X-ray map image elaboration

Analytical procedure

Analyses and observations at micrometer scale were performed in three distinct domains hosting garnet porphyroblasts which were chosen to acquire Si-Ti-Al-Fe-Mg-Mn-Ca-Na-K X-ray maps useful to highlight compositional variations associable to specific metamorphic reactions.

Spot chemical data were then used to compute mineralogical formulae by means of Minpet 2.02 software (Richard 1995) on the basis of 6 oxygens for ilmenite, 8 oxygens for feldspars, 22 oxygens for white mica and 36 oxygens for chlorite. Garnet formulae were calculated on the basis of 12 oxygens and 8 cations, considering all iron as FeO, in order to allow comparison of the obtained spot chemical analyses with the garnet compositions modeled through the available solid solution model used for P-T pseudosection computation, that does not include the andradite end-member (Powell and Holland 2008). Used mineral abbreviations are after Kretz (1983), reviewed by Siivola and Schmid (2007) (see Appendix A for device characteristics and representative analyses).

Following the methodological approach of Launeau et al. (1994), X-ray maps of the three selected domains were elaborated to obtain high contrast pseudocolor images by means of multichannel classification procedure, here implemented with the image processing tools contained in the open source software with public license GRASS in its last release (i.e. 6.4.1). This operative procedure has the purpose of extracting quantitative information from classified images by means of a stepwise-controlled procedure, as reported in the flowchart of Fig. 4 (see Appendix B for further details).

During the first step, obtained pseudocolor maps were elaborated in order to: i) identify mineral phases up to few micrometers in size, such as inclusion trail phases and very fine-grained retrograde aggregates (e.g. leucoxene after ilmenite), ii) define modal abundances of all rock-forming minerals constituents, iii) better define the textural relationships between the mineral constituents. In the second step, image processing was performed exclusively on the garnet crystals of the three sites with the purpose of detecting mineral zoning developed during growth at variable P-T conditions.

Results

Garnet shows a prevalent almandine composition, in the range $Alm_{64}Sps_{17}Grs_{14}Prp_5$ (inner-core) and $Alm_{69}Sps_{15}Grs_{11}Prp_5$ (outer-core) to $Alm_{75}Sps_{13}Grs_6Prp_6$ (rim), with higher almandine and slightly lower spessartine towards rims (Fig. 5), suggesting weak temperature increase during crystal growth.

Ilmenite is characterized by a limited solid solution towards pyrophanite end-member with Mn content (Mn/(Mn+Fe+Mg)) ranging from 0.050 to 0.075 (Fig. 5). Analyses carried out on leucoxene, formed as a widespread retrograde phase after ilmenite, give almost pure rutile composition (Fig. 5).

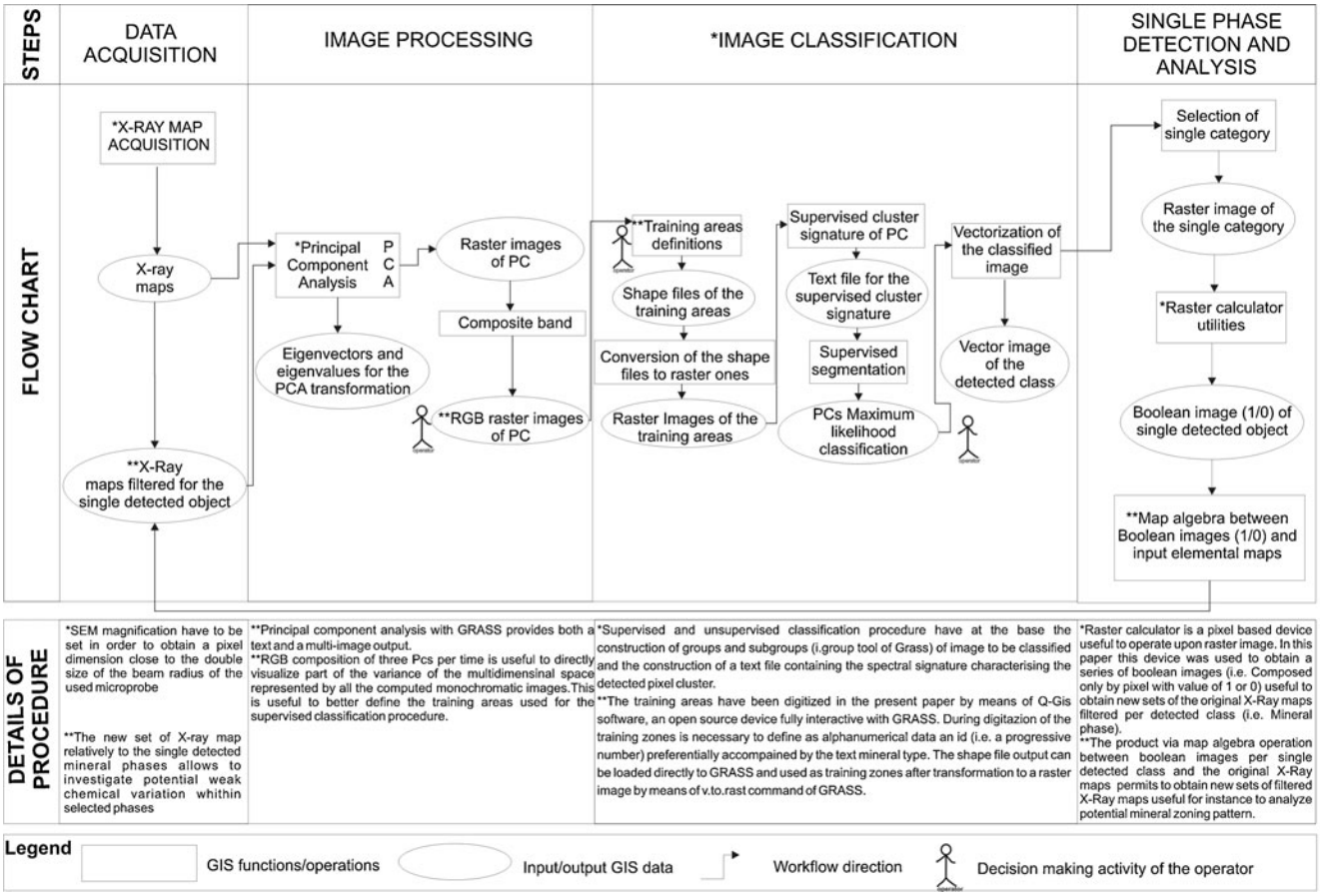

Fig. 4 Flowchart of the stepwise procedure used for image processing of X-ray maps via GIS based tools (GRASS 6.4.1)

White mica is a muscovite with moderate phengite content, with Si a.p.f.u. ranging from 3.08 to 3.28 (Fig. 5).

Chlorite compositions plot in the ripidolite field of the (Fe^{2+}+Fe^{3+}) *vs* Si diagram with a Fe/(Fe+Mg) ratio ranging from 0.64 to 0.67 (Fig. 5).

Pure albite forms the bulk of the plagioclase grains; the rare porphyroblasts show an oligoclase rim, with average composition An=17.2 % (Fig. 5).

BSE imaging and X-ray map analysis of the three selected domains (Fig. 6) confirm that garnet porphyroblasts started to grow during M_2 event, responsible for the formation of the S_2 surface, continuing to grow up to the later stages of this metamorphic event. Mn and Fe X-ray maps qualitatively confirm chemical variation during garnet growth as well as the appreciable compositional shift of ilmenite toward pyrophanite end-member. Ca X-ray maps illustrate the distribution of fluoroapatite, while the Mg ones well depict microfolded chlorite domains. K and Al X-ray maps reveal white mica distribution, while Na X-ray maps emphasize the location of albite crystals.

Following the proposed procedure for the image processing of X-ray maps of the selected micro-domains, multivariate statistical analysis via principal component computation (Launeau et al. 1994; Carr 1998) was first used to minimize the redundancy of data channels, permitting to better separate the contribution of the constituent mineral phases. After this step, maximum likelihood classification of all the principal components by means of supervised classification procedure (Flesche et al. 2000; Friel and Lyman 2006) allowed to pinpoint the modal percentage of the single phases in each analyzed domain, as well as to better define porphyroblast-matrix relationships in the studied rock (Fig. 7) (see Appendix B for further details).

Furhermore this procedure helped to confirm that inclusions of quartz, fluoroapatite and ilmenite depict an internal foliation within garnet porphyroblasts consistent with a syn-kinematic crystallization of these three mineral phases, in equilibrium with external albite. Chlorite is often in decussate aggregates mimicking the original S_1 surface. This may suggest former presence of prograde biotite, now entirely replaced by chlorite. White mica is instead preferentially located in the garnet pressure shadows crystallizing along the incipient formation of the S_3 surface.

Extraction of a new set of X-ray maps of the sole garnet via map algebra operation obtained with GRASS, allowed to obtain detailed growth zoning patterns (Fig. 8) highlighting the existence of a progressive chemical change during continuous garnet growth with changing of P-T conditions. This new

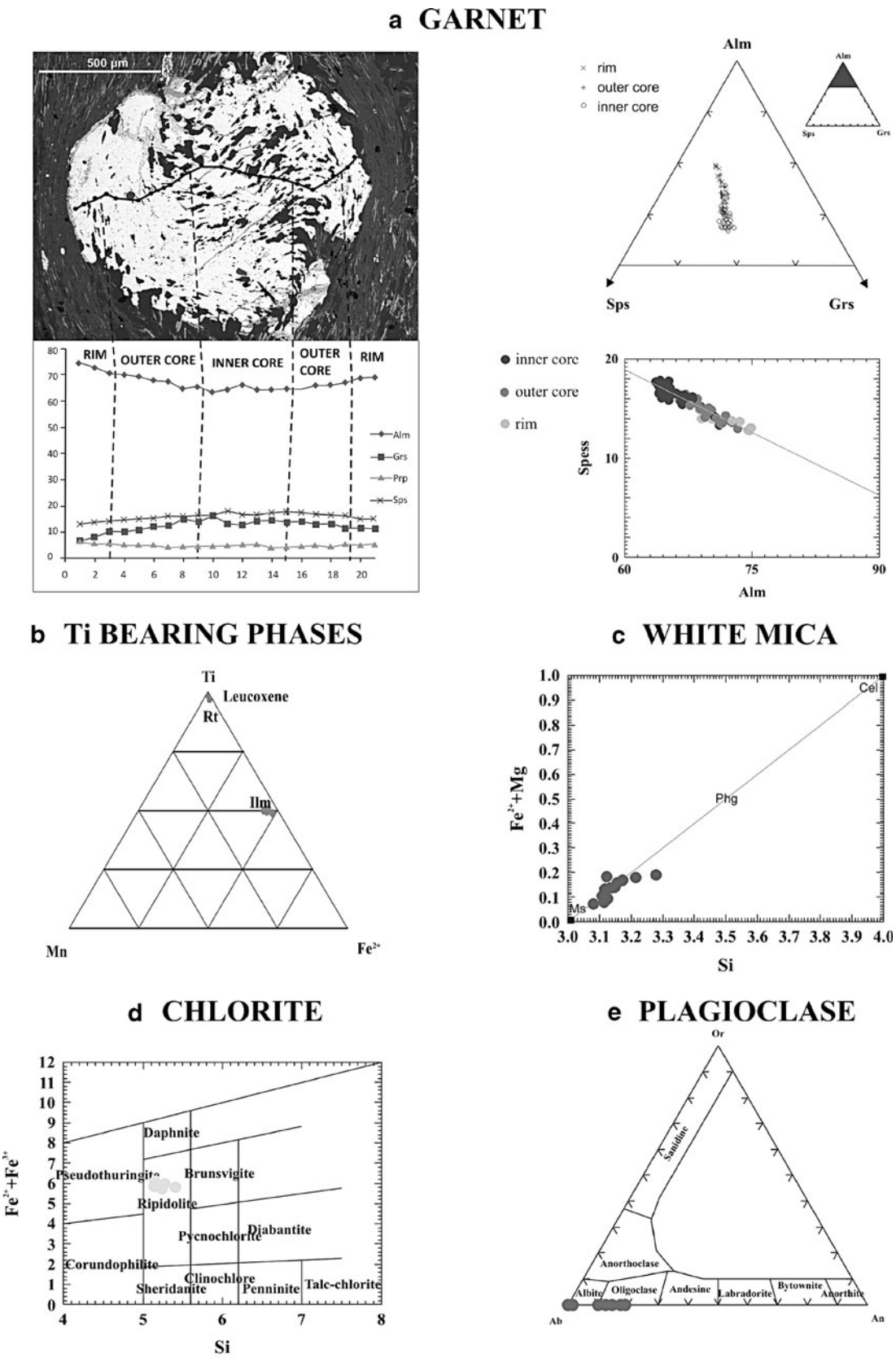

Fig. 5 Minerochemical features of the major mineral phases: **a**) composition profile and chemical compositions of garnet; **b**) ternary classification diagram for Ti-bearing phases; **c**) distribution of phengite content in white mica; **d**) classification diagram for chlorite; (**e**) ternary feldspar classification diagram

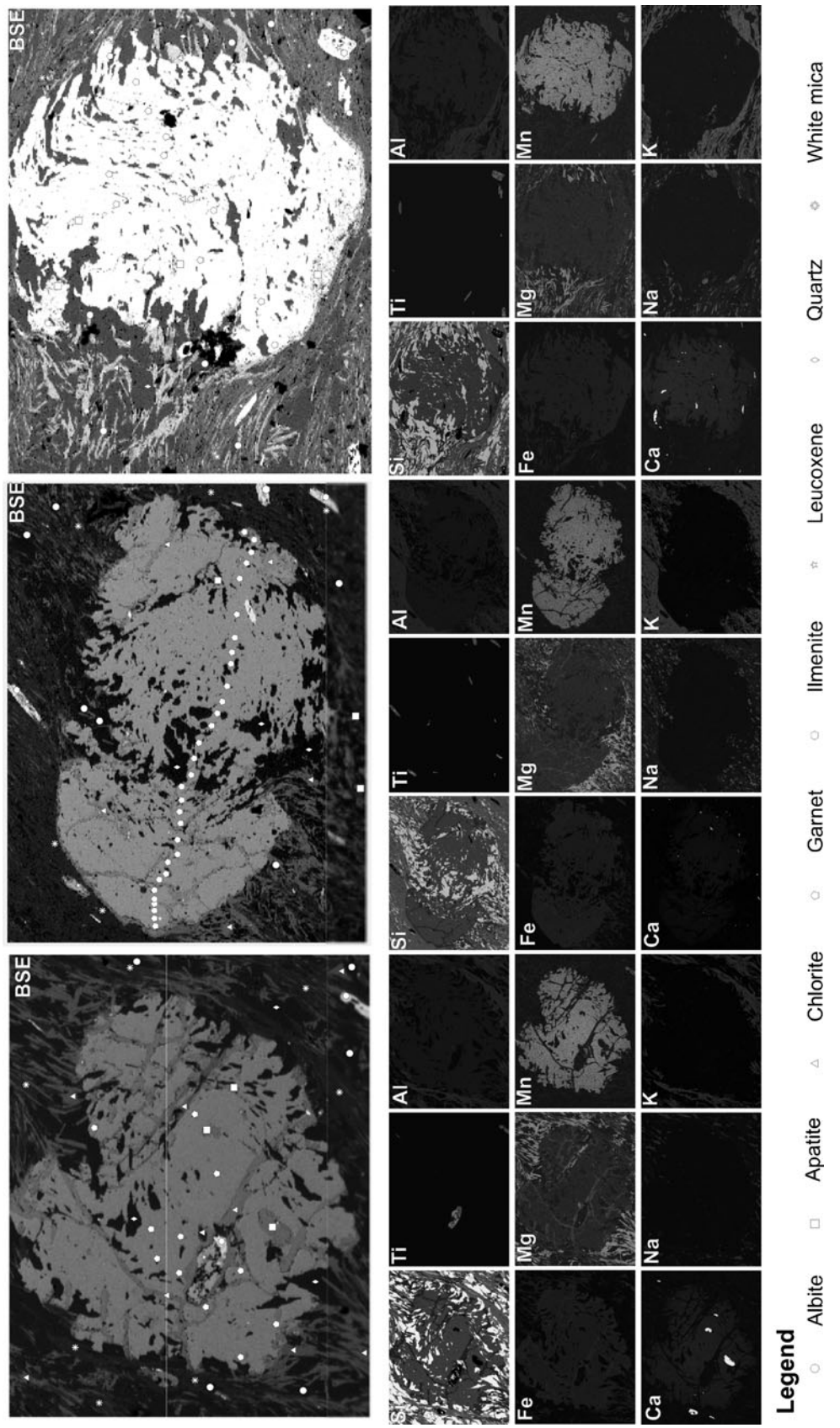

Fig. 6 Back scattered electron (BSE) images of the three selected garnet porphyroblastic domains, with location of spot analyses, and related elemental X-ray maps

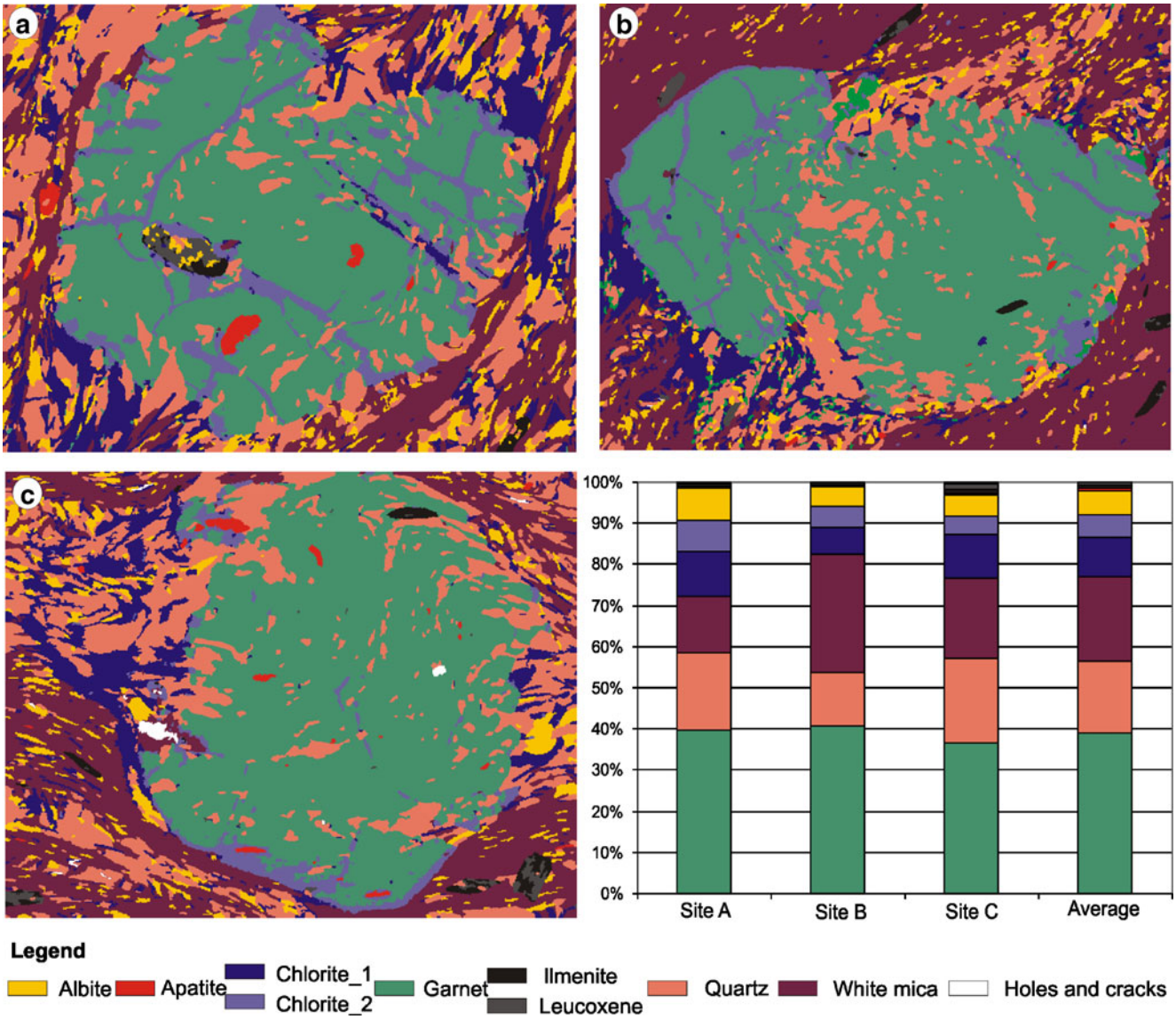

Fig. 7 Maximum likelihood classification obtained via principal component analysis of X-ray maps of the three selected garnet porphyroblastic domains with bar diagram of the computed volume percentage of detected mineral phases. Each image is composed of 512 columns×400 rows for an average pixel dimension of 2μm

visualization technique further permitted to emphasize the relative amounts of reactant garnet during the retrograde metamorphic evolutionary stages, and therefore to quantify the potential percentage of fractionated garnet after the attainment of the peak metamorphic stage (Appendix B).

Reconstruction of the P-T evolution

Methodological approach

The P-T trajectory of the selected upper greenschist facies ilmenite-garnet-bearing metapelite of the Mandanici Unit has been reconstructed by calculation of P-T pseudosections, that represent total phase diagrams sections for specific bulk-rock compositions (Will 1988). They are based on the composition of the "equilibrium volume": volume that contains those minerals that are interpreted to have once been in equilibrium with each other (i.e. paragenesis) (Powell and Holland 2008). According to Stüwe (1997), mineral parageneses can be directly derived using the bulk rock chemistry, or an effective bulk rock composition obtained excluding from the calculation those inner portions of porphyroblastic minerals affected by chemical fractionation from the syn-reacting mineral assemblage (Stüwe 1997; Evans 2004). The use of fixed bulk compositions in the pseudosection calculations implies indeed that the chemical systems in question are considered in overall equilibrium. This condition is fulfilled as long as no

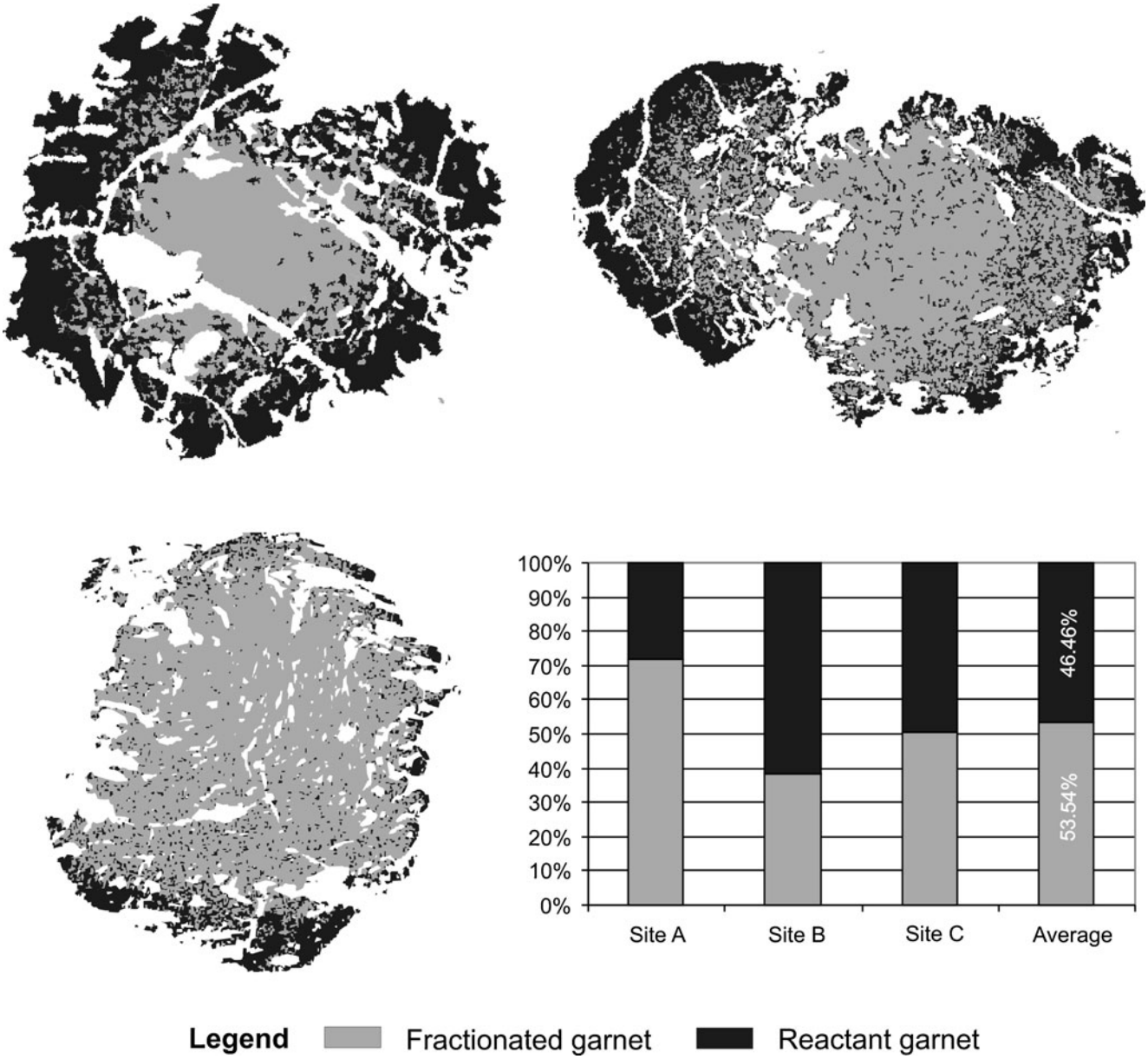

Fig. 8 Maximum likelihood classification obtained via principal component analysis of filtered garnet X-ray maps with bar diagram of volume percentage of fractionated and reactant garnet

chemical fractionation occurs, as a consequence of the multi-stage growth of some porphyroblastic minerals, since that results in the activation of an effective bulk composition (Stüwe 1997) operating during metamorphic evolution. Occurrence of mineral fractionation can be assessed through inconsistency between calculated and observed mineral equilibria, as for instance evidenced by the lack of intersection at least of three garnet compositional isopleths (e.g., almandine, grossular, and spessartine) within a relatively small area in the pseudosection P-T space (Evans 2004).

In these cases, the volumes of fractionated phases can be estimated, by means of quantitative compositional maps analysis, capable to constrain the real equilibrium volume and then the correct chemical analysis to be used for inferring the P-T constraints.

Taking into account the above mentioned methodology limits (e.g. Hetherington and Le Bayon 2005; Le Bayon et al. 2006; Caddick and Thompson 2008; Cirrincione et al. 2008; Angì et al. 2010; Groppo and Castelli 2010), pseudosections allow P-T path segments to be determined, by interpreting mineral proportions and compositional evolving trends. Perple_X is a software package that permits pseudosections to be calculated, on the basis of free energy minimization approach (Connolly 1990; Connolly and Petrini 2002). P-T conditions estimate depends on field position corresponding to observed assemblage in P-T space and on

isopleths (i.e. chemical iso-compositional curves) intersections. The obtained constraints may be considered reliable only if a good match between observed and calculated mineralogical assemblages is verified (e.g. Connolly and Petrini 2002; Cirrincione et al. 2008).

P-T pseudosections

A first P-T pseudosection for the selected sample was calculated using the July 2011 upgraded version of Perple_X (Connolly http://www.perplex.ethz.ch/) in the range T= 400–550 °C and P=0.20–1.00 GPa, considering: **1)** a closed-system behavior in the model chemical system TiO_2–MnO-Na_2O–CaO-K_2O–FeO–MgO-Al_2O_3-SiO_2-H_2O (TiMnNCKFMASH), suitable to exemplify the real system, which contains Ti in widespread ilmenite and Mn in garnet and ilmenite. **2)** SiO_2 in excess, as well as H_2O which also represents the only fluid phase, in agreement with the observed blastesis of hydrous mineral phases and the lack of carbonate ones; **3)** the internally consistent thermodynamic database of Holland and Powell (1998, their upgrade 2002; **4)** the Compensated Redlich Kwong (CORK) fluid equation of state of Holland and Powell (1991; 1998); **5)** the XRF composition as the effective bulk rock chemistry; 6) the following solid solution models: i) the Ti-bearing biotite of White et al. (2007) with DQF corrections to annite; ii) a quaternary garnet model (Holland and Powell 1998) with a restricted subdivision range on Mn 0 %<X<20 %; iii) the chlorite model of Holland et al. (1998); iv) the white mica model of Coggon and Holland (2002) revised by Auzanneau et al. (2010); Ti-phengite was excluded from the calculation because not considered a reliable substitution at the relatively low pressure conditions of the given system; v) a binary plagioclase solid solution (Newton et al. 1980); vi) the Fe-Mg-Mn staurolite after Holland and Powell (1998); vii) an ideal Mg-Fe-Mn chloritoid model with restricted range of X (Mn) up to 20 % (White et al. 2000); viii) an ideal ilmenite-geikielite-pyrophanite solid solution; see the Perple_X web site for further details (http://www.perplex.ethz.ch/PerpleX_solution_model_glossary.html)

The first calculated pseudosection reveals that almandine increment is mainly controlled by increasing temperature, spessartine component increases with decreasing pressure and temperature, grossular component increases with decreasing temperature and increasing pressure. The pyrophanite component increase is mainly related to decreasing temperature, contrary to the pure ilmenite component. Finally, the increase of phengite content in white mica is directly related to pressure increase while Fe/(Fe+Mg) ratio in chlorite decreases with temperature increase (Fig. 9).

The modeled isopleths closer to garnet inner core compositions ($Alm_{64}Sps_{17}Grs_{14}Prp_5$) generate intersections in a small region, characterized by T=515±5 °C and P=0.93± 0.03 GPa. This area also comprises pyrophanite isopleths (Mn/(Mn+Mg+Fe)=0.05 to 0.75), related to chemical re-equilibration of ilmenite porphyroblasts during syn-M_2 garnet core growth. Outer core garnet isopleth intersections ($Alm_{69}Sps_{15}Grs_{11}Prp_5$) provided comparable P-T estimates of T~525 °C and P~0.93 GPa, connected to a later phase of the same metamorphic event. The small area depicted by garnet rim isopleths intersections ($Alm_{75}Sps_{13}Grs_6Prp_6$; Fig. 9) indicates that the final garnet growth stages took place in equilibrium with the bulk rock composition and provides further P-T constraints (T~540 and P~0.803 GPa), highlighting a prograde evolution, during which crenulation schistosity obliterated most of the previous foliation. All isopleth intersections fall into the Bt+Chl+Wmca+Ilm+Grt pseudosection P-T field, in agreement with the observed equilibrium mineralogical assemblage, except for biotite, which was likely replaced by chlorite during retrogression. Obtained P-T estimates indicate greenschist-amphibolite facies boundary conditions. Retrograde evolution produced blastesis of oligoclase in textural equilibrium with chlorite, formed at expense of biotite and/or garnet as pseudomorphs and reaction rims, leucoxene replacing ilmenite and white mica III with phengite intermediate content. This assemblage did not provide any useful intersection in the pseudosection P-T space (Fig. 9) highlighting the fact that the equilibrium volume represented by this mineral paragenesis resulted in disequilibrium with the used XRF bulk rock chemistry.

In this view, according to the procedure developed by Zuluaga et al. (2005), the molar amount of oxides fractionation responsible for the effective bulk rock chemistry shift was calculated, considering garnet and ilmenite as the only mineral phases involved in the fractionation process. The amount of ilmenite fractionation was computed considering the relative percentage of unaltered ilmenite (0.61 % vol; Appendix B) and retrograde leucoxene (0.72 % vol; Appendix B) quantified by means of the image classification of the three selected porphyroblastic domains (Fig. 7). This implies that about 46 % of Ti-bearing phases was likely subtracted from the retrograde reacting assemblage. Since the total amount of these phases accounts for the 1.4 % average volume in the whole sample (Fig. 3), it follows that the total volume of fractionated ilmenite is equal to 0.64 %.

In order to obtain the volume of fractionating garnet, a second set of X-ray maps, portraying only the three garnet porphyroblasts, was elaborated by means of multivariate statistical analysis (Fig. 8) allowing to detect and quantify the intra-garnet chemical variations not identifiable throughout the first image processing step. Taking into account that the total modal percentage of garnet is of 1.7 % (Fig. 3), this value was corrected subtracting the calculated relative percentage of fractionated garnet not involved in the retrograde reactions, estimated by means of the image processing procedure (light-gray regions in Fig. 8). Being the relative

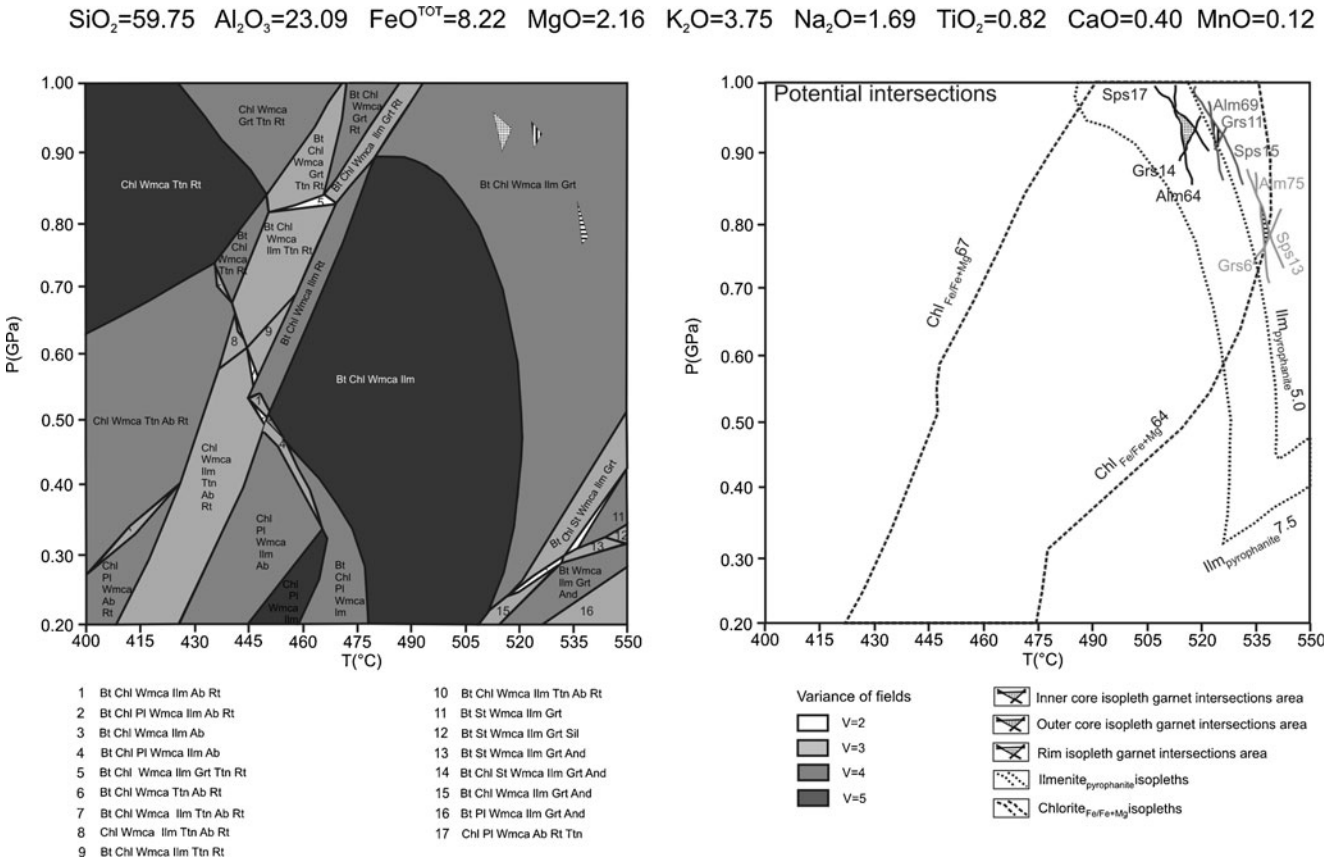

Fig. 9 *P-T* pseudosection calculated in the TiMnNCKFMASH model system using equilibrium rock composition obtained via XRF bulk-rock analysis

average percentage of retrograde reactant garnet of about 46 %, this implies that the fractionated garnet accounts for a total modal abundance of about 0.9 %.

The chemical fractionation effects to be subtracted from the XRF bulk rock chemistry (Table 1) were therefore calculated, taking into account the contributions of ilmenite and garnet by using two different density correction factors, both calculated at the same P-T values estimated for peak metamorphic conditions. The density ratio between ilmenite and whole rock allowed to extract a correction factor of 1.65, providing the reactant retrograde bulk rock chemistry due to ilmenite fractionation effects (Table 1). The second density ratio correction factor, between garnet and whole rock, allowed to extract a correction factor of 1.45, which permitted to add also the contribution due to garnet fractionation, providing a realistic molar correction of the reactant retrograde bulk rock chemistry (Table 1). The corrected composition shows that MnO disappears, TiO_2 content is significantly reduced in the new effective bulk rock chemistry, while some decrease in Al_2O_3 and FeO as well as an increase in SiO_2 and MgO can be observed.

The newly obtained equilibrium chemical system TiO_2-Na_2O-CaO-K_2O-FeO-MgO-Al_2O_3-SiO_2-H_2O (TiNCKFMASH) is considered to represent the observed retrograde chemical equilibria. Also in this case SiO_2 and H_2O were considered to be in excess and the same fluid equation of state and the internally consistent thermodynamic database of Holland and Powell (1991; 1998), as well as the already mentioned solid solution models were used for calculation.

The pseudosection, calculated taking into account the fractionation effects, revealed a simpler topology. Chemical isopleths in this pseudosection P-T space permitted to ascertain a significant increment of the plagioclase anorthite content, mainly controlled by decompressional effects, and an increment of white mica phengite content with pressure increase (Fig. 10). The observed compositional ranges of anorthite (An_{15-19}) and phengite (Phg_{12-18}), consistent with the retrograde compositional equilibrium, also characterized by the presence of retrograde rutile (i.e leucoxene) and chlorite, permitted to constrain a relatively large pseudosection P-T space with temperature ranging between 420 and 460 °C and pressure of 0.30–0.60 GPa, suggesting a low greenschist facies retrograde stage. The computed assemblage (i.e. Bt+Chl +Wmca+Pl+Ab+Rt) fits well the observed paragenetic equilibria except for the presence of Bt, not observed in our sample.

Discussion and conclusion

Thermodynamic modeling of metapelitic systems has been affirmed as a routinely performed method for unraveling the

Table 1 Calculation of amount of oxides to be fractionated from ilmenite+garnet porphyroblasts

Ilmenite density	4,715 Kg/m^3									
Rock density	2,855 Kg/m^3									
Density ratio	1,65									
Fractionated ilmenite mode	0,64 %									
Oxides	SiO_2	TiO2	Al_2O_3	FeO	MgO	MnO	CaO	Na_2O	K_2O	TOTAL
Ilmenite average composition (wt%)	0,00	53,07	0,00	43,03	0,00	3,91	0,00	0,00	0,00	100,00
Normalized to 100	0,00	53,07	0,00	43,03	0,00	3,91	0,00	0,00	0,00	100,00
Fractioned ilmenite deduction (0.64 % mode adjustment ratio)	0,00	0,56	0,00	0,45	0,00	0,04	0,00	0,00	0,00	1,06
Bulk rock chemistry (wt%)	59,75	0,82	23,09	8,22	2,16	0,12	0,40	1,69	3,75	100,00
Normalized to 100	59,75	0,82	23,09	8,22	2,16	0,12	0,40	1,69	3,75	100,00
Bulk rock chemistry (wt%) normalized to 100—fractioned ilmenite deduction	59,75	0,26	23,09	7,77	2,16	0,08	0,40	1,69	3,75	98,94
Normalized to 100	60,39	0,26	23,34	7,85	2,18	0,08	0,40	1,71	3,79	100,00
Oxides molar weights	60,09	79,88	101,94	71,85	40,32	70,94	56,08	61,98	94,20	
Molar proportions	1,00	0,00	0,23	0,11	0,05	0,00	0,01	0,03	0,04	1,48
Normalized to 100: molar proportions after ilmenite fractionation	68,06	0,22	15,50	7,40	3,67	0,08	0,49	1,87	2,72	100,00
Garnet density	4,715 Kg/m^3									
Rock density	2,855 Kg/m^3									
Density ratio	1,45									
Fractionated garnet mode	0.9 %									
Oxides	SiO_2	TiO2	Al_2O_3	FeO	MgO	MnO	CaO	Na_2O	K_2O	TOTAL
Garnet inner core composition (wt%)	38,59	0,00	21,07	28,26	1,05	7,01	4,29	0,00	0,00	100,27
Normalized to 100	38,49	0,00	21,01	28,18	1,05	6,99	4,28	0,00	0,00	100,00
Fractioned garnet deduction (0.9 % mode adjustment ratio)	0,50	0,00	0,27	0,37	0,01	0,09	0,06	0,00	0,00	1,31
Bulk rock chemistry (wt%)	68,06	0,22	15,50	7,40	3,67	0,08	0,49	1,87	2,72	100,00
Normalized to 100	68,06	0,22	15,50	7,40	3,67	0,08	0,49	1,87	2,72	100,00
Bulk rock chemistry (wt%) normalized to 100—fractioned garnet deduction	67,55	0,22	15,23	7,03	3,65	−0,02	0,43	1,87	2,72	98,70
Normalized to 100	68,27	0,22	15,39	7,10	3,69	−0,02	0,44	1,89	2,75	100,00
Oxides molar weights	60,09	79,88	101,94	71,85	40,32	70,94	56,08	61,98	94,20	
Molar proportions	1,14	0,00	0,15	0,10	0,09	0,00	0,01	0,03	0,03	1,55
Normalized to 100: molar proportions used to calculate the pseudosection of Fig.11	73,41	0,18	9,76	6,39	5,92	−0,01	0,50	1,97	1,89	100,00

P-T evolution of metamorphic complexes. Nevertheless, a correct definition of the system parameters is not always straightforward due, for instance, to the difficulty in defining the real reacting equilibrium volume. Therefore, in this study, multispectral statistical image analysis has been applied to X-ray maps in order to minimize the operator subjectivity in the identification of equilibrium assemblages.

This paper provides the first detailed tectono-metamorphic reconstruction for the greenschist facies basement of the Peloritani Mountains, obtained through geothermobarometric modeling assisted by image data handling, via principal component analysis, of a fine-grained porphyroblastic metapelite from the Mandanici Unit. The used methodological approach is well suited to reliably reconstruct the porphyroblast-matrix relationships and therefore to better define both the succession and P-T conditions of the deformational and metamorphic events. Furthermore this method has proven to be a particularly powerful tool for quantifying the volumetric amounts of minerals that continue to participate in metamorphic reactions after fractionation of their inner portions.

The selected rock sample, whose mineralogical assemblage comprises quartz+muscovite+chlorite+ilmenite+leucoxene/rutile+garnet±fluorapatite±monazite±zircon, shows mainly the paragenesis stable at peak or near-peak conditions, depicting a crenulation schistosity S_2 that largely obliterates the former schistosity S_1. Retrograde evolution is mostly represented by the breakdown of garnet and ilmenite, replaced by chlorite and leucoxene/rutile, respectively, and by development of a S_3 mylonitic schistosity locally preserved between fragments of pinch and swells garnet porphyroblasts.

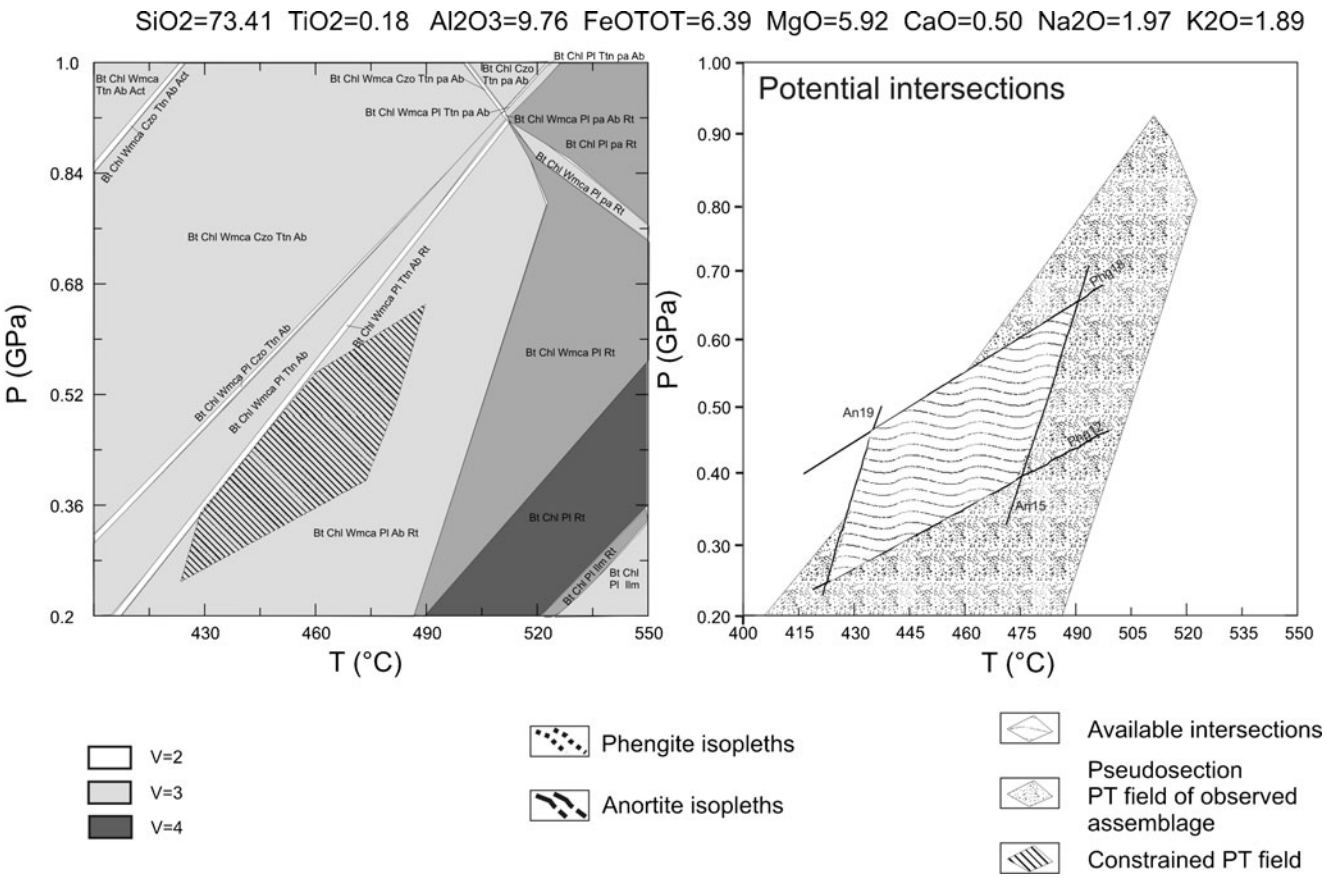

Fig. 10 P-T pseudosection calculated in the TiNCKFMASH model system using equilibrium rock composition obtained via fractionation method (Zuluaga et al. 2005; modified) assisted by image processing results as illustrated in Figs. 7 and 8 (see text for explanation)

Through a microstructural analysis especially focused on garnet porphyroblast microstructures, metamorphic-deformational relationships were reconstructed. Garnet recorded the second and third deformational event: cores with quartz and ilmenite inclusions exhibit a folding pattern linked to D_2, indicating nucleation of the porphyroblast cores during the early stages of the second metamorphic event. The later stages of M_2 is also responsible for unfolded rims over growing the crenulated cores. D_3 produced stretching, testified by local pinch-and-swell structures and porphyroclasts rotation.

Garnet porphyroblasts gave essential information not only about the sequence of the deformational stages, but also about the changing metamorphic conditions. X-ray maps and compositional transects crossing rim, outer-core and inner-core of the investigated pophyroblasts revealed a growth-zoning pattern, from $Alm_{64}Sps_{17}Grs_{14}Prp_5$ (inner-core) and $Alm_{69}Sps_{15}Grs_{11}Prp_5$ (outer-core) to $Alm_{75}Sps_{13}Grs_6Prp_6$ (rim), with spessartine decreasing towards rims in favor of almandine. Furthermore, image analysis of X-ray maps, allowed to better define location and mutual textural relationships between garnet and ilmenite porphyroblasts, inclusion trails and matrix minerals, as well as to emphasize the geometry of the elemental composition distribution within garnet porphyroblasts, useful for the correct interpretation of the minerochemical data.

A recent version of the Perple_X phase diagram computation software package allowed to calculate a P-T pseudosection in the TiMnNCKFMASH system, able to define also the thermodynamic behavior of ilmenite that played a significant role in Mn-exchange reactions and resulted therefore very useful to further refine the P-T estimates. As a whole, garnet and ilmenite inclusion isopleths intersections allowed peak conditions (T~540 °C and P~0.8 GPa) to be determined.

In more detail, isopleths referred to garnet inner-core and pyrophanite isopleths indicate T~515 °C and P~0.93 GPa (baric peak), confirming that ilmenite was likely re-equilibrated during nucleation of garnet.

Outer core garnet isopleths intersections gave T~525 °C and P~0.93 GPa. By integrating microstructural and chemical data, these P-T estimates can be referred to the first metamorphic stage associated to isoclinalic folding. Rim garnet isopleths intersections provided T~540 °C and P~0.80 GPa, representing metamorphic peak conditions, associated to the development of the crenulation schistosity. Retrograde P-T trajectory was finally determined after quantification of the chemical fractionation effects, caused by progressive

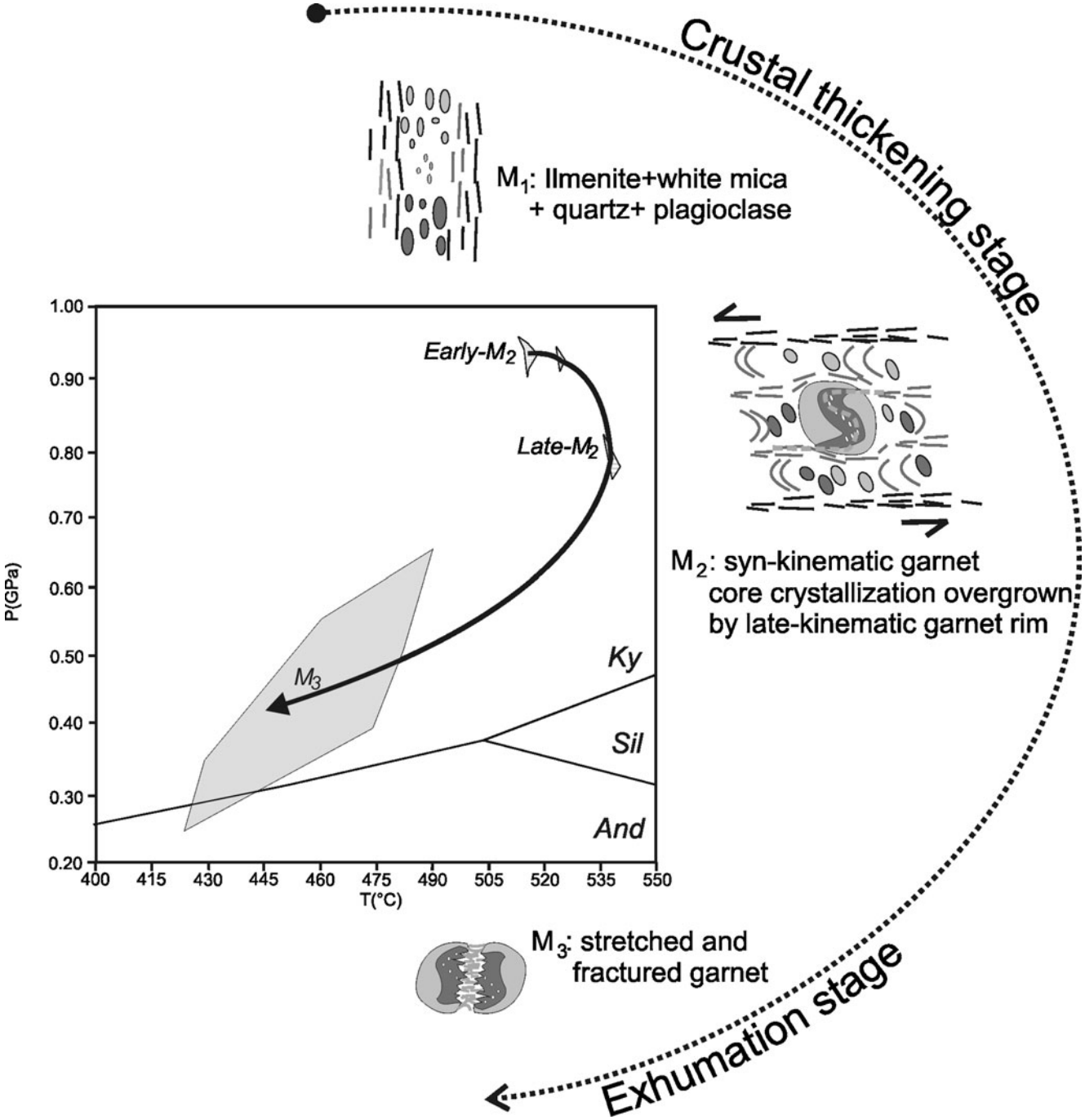

Fig. 11 Comprehensive P-T path including all the reconstructed tectono-metamorphic events

depletion of specific chemical constituents sealed in the inner portions of the crystals during early garnet growth stages, as well as in ilmenite portions not affected by retrogression to leucoxene. This permitted to calculate the new effective bulk rock chemistry operating during the retrograde metamorphic evolution and to obtain P-T pseudosection stability fields consistent with the observed retrograde parageneses.

Chemical isopleths in this P-T pseudosection permitted to ascertain a significant increment of the anorthite content in plagioclase, mainly controlled by decompressional effects, and an increment of the phengite content in white mica with pressure increase (Fig. 10). Observed compositional ranges of anorthite ($An_{15\text{-}19}$) and phengite content ($Phg_{12\text{-}18}$), coherent with the retrograde compositional equilibrium, allowed to constrain a relatively large pseudosection P-T space with temperature ranging between 420 and 460 °C and pressure of 0.30–0.60 GPa, coherent with a lower PT, greenschist-facies, retrograde stage.

The reconstructed pressure-temperature path (Fig. 11) depicts a typical clockwise P-T evolution. The prograde stage, peaking at boundary P-T conditions between greenschist and amphibolite facies, involved burial at middle-lower levels during crustal thickening, possibly connected to Hercynian continental collision processes. The following retrograde evolution took place under lower greenschist facies conditions, during a late- to post-orogenic shearing stage likely related to late Hercynian exhumation.

The obtained results introduce an element of great novelty to the geological knowledge of the Peloritani Mountains. Indeed, the basement rocks forming the Mandanici and Aspromonte-Peloritani Units have been up to now considered integral parts of the same chain sector developed at upper and middle crust conditions, respectively. The relatively high pressure values of ~0.93 GPa recorded by the studied metapelite sample highlight, on the contrary, that lower crustal conditions were attained by the rocks of the Mandanici Unit during their orogenic evolution.

It is demostrated in this study that new integrated techniques as the ones used are very powerful in reconstructing longer segments of a polyphase evolution in more detail, including reliable identification of both baric and thermal peak conditions, and have therefore provide much stronger constraints for the reconstruction of the tectono-metamorphic and geodynamic history of the mountain belts. These results open the way for a general review of previous interpretations on the crustal evolution of the chain sectors cropping out in the southern CPO, in the light of the highest potentialities offered by the new petrological techniques.

Acknowledgements We would like to thank C. Groppo for support with mineral chemical analyses and L. Zappalà for computer assistance during image processing of X-ray maps. We wish to thank the associate editor Georg Hoinkes and two anonymous reviewers for their careful and constructive reviews that have been very helpful in improving the manuscript. This work was supported by P.R.I.N. 2009 (research project grant by the Italian MIUR); project title: Tectono-metamorphic evolution of the crystalline basement units of the eastern sector of the Rhodope Massif.

APPENDIX A. Representative analyses of mineral phases and micro-analytical device features

Table 2 Mineral chemical analyses

Representative mineral analyses of garnet						
Zone	Inner core		Outer core		Rim	
SiO_2	38.67	36.17	38.42	38.07	36.34	37.95
Al_2O_3	21.26	19.93	20.77	21.27	20.11	21.25
FeO^{tot}	27.24	29.69	29.42	28.58	31.99	31.85
MnO	7.00	7.71	6.53	6.78	6.64	5.47
MgO	1.11	0.71	1.19	1.32	0.89	1.37
CaO	4.72	4.82	3.67	3.99	3.69	2.12
Total	100.00	99.03	100.00	100.01	99.66	100.01
Si	3.121	2.976	3.113	3.076	2.976	3.080
Al^{IV}	0.000	0.024	0.000	0.000	0.024	0.000
Sum_T	3.121	3.000	3.113	3.076	3.000	3.080
Al^{VI}	2.021	1.908	1.982	2.024	1.916	2.031
Sum_A	2.021	1.908	1.982	2.024	1.916	2.031
Fe^{2+}	1.838	2.043	1.994	1.931	2.191	2.162
Mg	0.134	0.087	0.144	0.159	0.109	0.166
Mn	0.478	0.537	0.448	0.464	0.461	0.376
Ca	0.408	0.425	0.319	0.345	0.324	0.184
Sum_B	2.859	3.092	2.904	2.900	3.084	2.888
Sum_cat	8	8	8	8	8	8
# of oxygens	12	12	12	12	12	12
Alm	64.31	66.07	68.65	66.60	71.04	74.86
Grs	14.28	13.74	10.97	11.91	10.50	6.38
Sps	16.74	17.38	15.43	16.00	14.94	13.02
Prp	4.67	2.82	4.95	5.48	3.52	5.74
Representative mineral analyses of plagioclase						
Zone	Inner and outer core			Rim		
SiO_2	69.23	68.44	68.48	63.65	63.36	64.53

Table 2 (continued)

Al_2O_3	19.08	19.24	18.96	22.31	22.16	21.52
CaO	0.00	0.31	0.00	3.72	4.04	3.16
Na_2O	11.61	11.48	11.65	9.49	9.45	9.89
K_2O	0.00	0.00	0.00	0.00	0.00	0.00
Total	99.92	99.47	99.09	99.17	99.01	99.1
Si	3.019	3.002	3.020	2.842	2.828	2.8
Al	0.979	0.994	0.980	1.158	1.172	1.2
Ca	0.000	0.014	0.00	0.172	0.188	0.1
Na	0.981	0.976	0.980	0.819	0.811	0.8
K	0.00	0.00	0.00	0.00	0.00	
Ab	100	98.50	100.00	82.4	80.9	85.10
An	0.00	1.50	0.00	17.6	19.1	14.90
Or	0.00	0.00	0.00	0.00	0.00	0.00
Sum_cat	4.98	4.99	4.98	4.99	5.00	4.99
# of oxygens	8	8	8	8	8	8
Representative mineral analyses of white mica						
Zone	matrix		matrix		matrix	
SiO_2	45.37		45.89		45.56	
TiO_2	0.36		0.00		0.00	
Al_2O_3	34.09		33.24		33.44	
FeO^{tot}	1.33		1.69		1.32	
MnO	0.00		0.00		0.00	
MgO	0.24		0.43		0.45	
CaO	0.00		0.00		0.00	
Na_2O	1.16		1.19		1.37	
K_2O	8.32		8.45		8.68	
Total	95.17		95.26		95.20	
Si	3.109		3.155		3.148	
Al^{IV}	0.891		0.845		0.852	
Al^{VI}	1.905		1.867		1.871	
Ti	0.018		0.000		0.000	
Fe^{2+}	0.077		0.108		0.082	
Mn	0.000		0.000		0.000	
Mg	0.026		0.051		0.057	
Ca	0.000		0.000		0.000	
Na	0.153		0.161		0.186	
K	0.735		0.755		0.766	
Sum_cat	6.914		6.942		6.962	
# of oxygens	12		12		12	
XFe^{2+}	0.75		0.68		0.59	
Phg	10.9		15.5		14.8	
Representative mineral analyses of ilmenite						
Zone	within grt		matrix			
TiO_2	52.17	52.46	53.42	52.71		
Cr_2O_3	0.00	0.00	0.00	0.00		
FeO	46.20	44.23	44.12	42.64		
MnO	2.51	3.98	3.16	4.55		
MgO	0.00	0.00	0.00	0.00		
Total	100.88	100.67	100.7	99.9		
Ti	1.968	1.987	2.022	2.001		
Cr	0.000	0.000	0.000	0.000		

Table 2 (continued)

Fe	1.961	1.862	1.828	1.791
Mn	0.101	0.171	0.130	0.208
Mg	0.000	0.00	0.000	0.00
Sum_cat	4.03	4.01	3.98	4.00
# of oxygens	6.00	6.00	6.00	6.00
Mn/(Mg+Fe+Mn)	0.05	0.08	0.07	0.10
Fe/(Mg+Fe+Mn)	0.95	0.92	0.93	0.90
Representative mineral analyses of chlorite				
Zone	matrix	matrix	matrix	
SiO_2	23.75	23.18	23.16	
Al_2O_3	21.76	22.28	21.85	
TiO_2	0.00	0.00	0.00	
FeO	31.00	31.55	32.92	
MnO	0.34	0.00	0.00	
MgO	9.86	9.53	9.01	
Total	86.71	86.54	86.94	
Si	5.241	5.137	5.150	
Al^{IV}	2.759	2.863	2.850	
Al^{VI}	2.896	2.952	2.872	
Ti	0.000	0.000	0.000	
Fe^{2+}	5.721	5.847	6.122	
Mn	0.064	0.000	0.000	
Mg	3.244	3.148	2.987	
Sum_cat	19.925	19.947	19.981	
# of oxygens	36.00	36.00	36.00	
Al^{IV}/Al^{VI}	0.95	0.97	0.99	
XFe^{2+}	0.64	0.65	0.67	

Analysis and observations at micrometer scale were performed by TESCAN-VEGA\crLMU scanning electron microscope (SEM), at the Department of Biological, Geological and Environmental Science of Catania University, with backscattered electron mode, under high vacuum conditions at accelerating voltage 20 kV and beam current of 0.15 nA. The SEM was equiped with an EDS EDAX Neptune XM4 60, to provide chemical spot analysis

APPENDIX B. Multispectral image analysis outputs

Table 3 Quantitative output data of the three supervised image classifications and of the fractionated and reactant garnet proportions

Domains	Garnet 1		Garnet 2		Garnet 3		Average
Mineral	Pixel count	Cover %	Pixel count	Cover %	Pixel count	Cover %	Cover %
Quantitative output data of the three supervised image classifications							
Garnet	81530	39.81	83550	40.80	75324	36.78	39.13
Quartz	38245	18.67	26493	12.94	42027	20.53	17.38
White Mica	28204	13.78	59191	28.90	39898	19.48	20.72
Chlorite 1	22533	11.00	13244	6.46	21812	10.65	9.37
Chlorite 2	15108	7.38	10648	5.20	8970	4.38	5.65
Albite	16022	7.82	9427	4.60	10163	4.96	5.79
Ilmenite	870	0.42	1062	0.52	1809	0.88	0.61
Apatite	1349	0.66	913	0.45	1142	0.56	0.56
Leucoxene	939	0.46	272	0.13	3218	1.57	0.72

Table 3 (continued)

Domains	Garnet 1		Garnet 2		Garnet 3		Average
Mineral	Pixel count	Cover %	Pixel count	Cover %	Pixel count	Cover %	Cover %
Holes and cracks	0	0	0	0	437	0.21	0.07
Total	204800	100	204800	100	204800	100	100
Quantitative output data of the fractionated and reactant garnet proportions							
Fractionated garnet	31228	38.55	41543	50.38	54072	71.79	53.54
Reactant garnet	49770	61.45	41091	49.72	21252	28.21	46.46
Total	80998	100	82634	100	75324	100	100

Quantitative results of the maximum likelihood classification (MLC) obtained by principal component analysis (PCA) of the Si-Ti-Al-Fe-Mg-Mn-Ca-Na-K X-Ray maps. Image classification is based upon a preliminary statistical data manipulation of the pixel values of the elemental X-Ray maps via PCA, useful to minimize the redundancy of the multispectral images, (Launeau et al. 1994). This procedure permits to obtain a new set of multispectral images (e.g. PC images) better suited to discriminate and quantify the single mineral phases by operator-driven classification method. Each image is composed of 512 columns×400 rows of pixels (i.e. 204,800 pixels) for an average pixel dimension of 2 μm. Quantitative results of the maximum likelihood classification of the three filtered garnet porphyroblasts obtained by preliminary statistical data handling of Fe-Mg-Mn-Ca X-ray maps via PCA

References

Angì G, Cirrincione R, Fazio E, Fiannacca P, Ortolano G, Pezzino A (2010) Metamorphic evolution of preserved Hercynian crustal section in the Serre Massif (Calabria-Peloritani Orogen, southern Italy). Lithos 115:237–262

Appel P, Cirrincione R, Fiannacca P, Pezzino A (2011) Age constraints on Late Paleozoic evolution of continental crust from electron microprobe dating of monazite in the Peloritani Mountains (southern Italy): another example of resetting of monazite ages in high-grade rocks. Int J Earth Sci 100:107–123

Atzori P, Sassi FP (1973) The barometric significance of the muscovites from Savoca phyllites (Peloritani, Sicily). With considerations on the baric conditions during Hercynian metamorphism in Italy. Schweiz Miner Petr Mitt 53(2):243–253

Atzori P, Ferla P (1992) The pre-alpine crystalline basement of the Peloritani Mountains (Sicily): acquired knowledge and open questions. IGCP N° 276 Newsletters 5:311–320

Atzori P, Cirrincione R, Del Moro A, Pezzino A (1994) Structural, metamorphic and geochronogical features of the Alpine events in the south-eastern sector of the Peloritani Mountains (Sicily). Per Mineral 63:113–125

Auzanneau E, Schmidt MW, Vielzeuf D, Connolly JAD (2010) Titanium in phengite: a geobarometer for high temperature eclogites. Contrib Mineral Petrol 159:1–24

Caddick MJ, Thompson AB (2008) Quantifying the tectono-metamorphic evolution of pelitic rocks from a wide range of tectonic settings: mineral compositions in equilibrium. Contrib Mineral Petrol 156:177–195

Carr JR (1998) A visual basic program for principal components transformation for digital images. Comput Geosci 24:209–218

Cirrincione R, Pezzino A (1991) Caratteri strutturali dell'evento Alpino nella serie mesozoica di Alì e nell'Unità metamorfica di Mandanici (Peloritani Orientali). Mem Soc Geol It 47:263–272

Cirrincione R, Atzori P, Pezzino A (1999) Sub-greenschist facies assemblages of metabasites in South-Eastern sector of Peloritani range. Mineral Petrol 67:193–212

Cirrincione R, Ortolano G, Pezzino A, Punturo R (2008) Poly-orogenic multi-stage metamorphic evolution inferred via P–T pseudosections: an example from Aspromonte Massif basement rocks (Southern Calabria, Italy). Lithos 103:466–502

Cirrincione R, Fazio E, Ortolano G, Pezzino A, Punturo R (2012) Fault-related rocks as a tool for the comprehension of structural and metamorphic evolution of an accretionary wedge in a collisional belt (Peloritani Mountains, NE Sicily). Int Geol Rev 54:940–956

Coggon R, Holland TJB (2002) Mixing properties of phengitic micas and revised garnet-phengite thermobarometers. J Metam Geol 20:683–696

Connolly JAD (1990) Multivariable phase diagrams: an algorithm based on generalized thermodynamics. Am J Sci 290:666–718

Connolly JAD (2005) Computation of phase equilibria by linear programming: a tool for geodynamic modeling and its application to subduction zone decarbonation. Earth Planet Sci Lett 236:524–541

Connolly JAD (2009) The geodynamic equation of state: what and how. Geochem Geophys Geosyst 10:Q10014. doi:10.1029/2009GC002540

Connolly JAD, Petrini K (2002) An automated strategy for calculation of phase diagram sections and retrieval of rock properties as a function of physical conditions. J Metam Geol 20:697–708

De Gregorio S, Rotolo SG, Villa IM (2003) Geochronology of the medium to high grade metamorphic units of the Peloritani Mts., Sicily. Int J Earth Sci 92:852–872

De La Roche H (1978) La chimique des roches présentée et interpretée d'aprés la structure de leur faciés mineral dans l'espace des variables chimiques: function spécifiques et diagrammes qui s'en déduisent. Application aux roches ignées. Chem Geol 21:63–87

Dubois R, Truillet R (1971) Le polymétamorphisme et la structure du domain peloritain (Sicile). La notion de socle peloritain antéhercynien. CR Acad Sci Paris 272:2134–2136

Evans TP (2004) A method for calculating effective bulk composition modification due to crystal fractionation in garnet-bearing schists: implications for isopleths thermobarometry. J Metam Geol 22:547–557

Ferla P (1972) Serie metamorfiche dei Monti Peloritani occidentali (Messina). Rend Soc Ital Min Petr 28:125–151

Ferla P (2000) A model of continental crustal evolution in the geological history of the Peloritani Mountains (Sicily). Mem Soc Geol It 55:87–93

Ferla P, Meli C (2007) Petrogenesis of tourmaline rocks associated with Fe-carbonate–graphite metapelite, metabasite and strata-bound polymetallic sulphide mineralisation, Peloritani Mountains, Sicily, Southern Italy. Lithos 99:266–288

Fiannacca P, Williams IS, Cirrincione R, Pezzino A (2008) Crustal contributions to Late-Hercynian peraluminous magmatism in the Southern Calabria–Peloritani Orogen, Southern Italy:

petrogenetic inferences and the Gondwana connection. J Petrol 49:1497–1514

Fiannacca P, Williams IS, Cirrincione R, Pezzino A (2012) The augen gneisses of the Peloritani Mountains (NE Sicily): granitoid magma production during rapid evolution of the northern Gondwana margin at the end of the Precambrian. Gondwana Res. doi:10.1016/j.gr.2012.05.019

Flesche H, Nielsen AA, Larsen R (2000) Supervised mineral classification with semi-automatic training and validation set generation in scanning electron microscope energy dispersive spectroscopy images of thin sections. Math Geol 32:337–366

Franzini M, Leoni L, Saitta M (1972) A simple method to evaluate the matrix effect in x-ray fluorescence analysis. XRay Spectrom 1:151–154

Friel JJ, Lyman CE (2006) X-ray mapping in electron-beam instruments. Microsc Microanal 12:2–25

Gaidies G, Abart R, De Capitani C, Schuster R, Connolly JAD, Reusser E (2006) Characterization of polymetamorphism in the Austroalpine basement east of the Tauern Window using garnet isopleth thermobarometry. J Metam Geol 24:451–475

Groppo C, Castelli D (2010) Prograde P-T evolution of a lawsonite eclogite from the Monviso meta-ophiolite (Western Alps): dehydration and redox reactions during subduction of oceanic FeTi-oxide gabbro. J Petrol 51:2489–2514

Herron MM (1988) Geochemical classification of terrigenous sands and shales from core and log data. J Sed Petrol 58:820–829

Hetherington CJ, Le Bayon R (2005) Bulk rock composition: a key to identifying invisible prograde reactions in zoned garnet. Swiss Bull Miner Petrol 85:57–68

Holland TJB, Powell R (1991) A compensated-Redlich-Kwong (CORK) equation for volumes and fugacities of CO_2 and H_2O in the range 1 bar to 50 kbar and 100–1600 °C. Contrib Mineral Petrol 109:265–273

Holland TJB, Powell R (1998) An internally consistent thermodynamic data set for phases of petrological interest. J Metam Geol 16:309–343

Holland TJB, Baker J, Powell R (1998) Mixing properties and activity-composition relationships of chlorites in the system MgO-FeO-Al_2O_3-SiO_2-H_2O. Eur J Mineral 10:395–406

Kretz R (1983) Symbols for rock-forming minerals. Am Mineral 68:277–279

Launeau P, Cruden AR, Bouchez J (1994) Mineral recognition in digital images of rocks; a new approach using multichannel classification. Can Mineral 32:919–933

Le Bayon B, Pitra P, Ballevre M, Bohn M (2006) Reconstructing P–T paths during continental collision using multi-stage garnet (Gran Paradiso nappe, Western Alps). J Metam Geol 24:477–496

Lentini F, Catalano S, Carbone S (2000) Carta geologica della Provincia di Messina (Sicilia Nord-Orientale), scala 1:50000, S.El.Ca, Firenze, p 70

Newton RC, Charlu TV, Kleppa OJ (1980) Thermochemistry of the high structural state plagioclases. Geochim Cosmochim Acta 44:933–941

Pezzino A, Pannucci S, Puglisi G, Atzori P, Ioppolo S, Lo Giudice A (1990) Geometry and metamorphic environment of the contact between the Aspromonte—Peloritani Unit (Upper Unit) and Madonna dei Polsi Unit (Lower Unit) in the central Aspromonte area (Calabria). Boll Soc Geol It 109:455–469

Pezzino A, Angì G, Cirrincione R, De Vuono E, Fazio E, Fiannacca P, Lo Giudice A, Ortolano G, Punturo R (2008) Alpine metamorphism in the aspromonte massif: implications for a new framework for the southern sector of the Calabria-Peloritani orogen, Italy. Int Geol Rev 50:423–441

Powell R, Holland TJB (2008) On thermobarometry. J Metam Geol 26:155–179

Puglisi G, Pezzino A (1994) Metamorphism in the central Aspromonte area: geological, mineralogical and petrogenetic relationships. Per Mineral 63:153–168

Raase P, Raith M, Ackermand D, Lal RK (1986) Progressive metamorphism of mafic rocks from greenschist to granulite facies in the Dharwar Craton of South India. J Geol 94:261–282

Richard LR (1995) Minpet mineralogical and petrological data processing system, version 2.02 Minpet Geological Software Quebec, Canada

Russo S, Cutrupia D, Di Bella M, Minutoli C (2006) High pressure metamorphism in southern Calabria, Italy: the Cardeto chlorite–garnet metapelites. Per Mineral 75:23–42

Siivola J, Schmid RA (2007) List of mineral abbreviations. In: Fettes D, Desmons J (eds) Metamorphic rocks—a classification and glossary of terms. Cambridge University Press, Cambridge, pp 93–110

Stüwe K (1997) Effective bulk composition changes due to cooling: a model predicting complexities in retrograde reaction textures. Contrib Mineral Petrol 129:43–52

Taylor SR, Mclennan SM (1985) The continental crust: its composition and evolution. Blackwell, Oxford, p 312

Will TM (1988) Phase diagrams and their application to determine pressure-temperature paths of metamorphic rocks. Neu Jahrb Miner Abh 174:103–130

Williams IS, Fiannacca P, Cirrincione R, Pezzino A (2012) Peri-Gondwanan origin and early geodynamic history of NE Sicily: a zircon tale from the basement of the Peloritani Mountains. Gondwana Res. doi:10.1016/j.gr.2011.12.007

White RW, Powell R, Holland TJB, Worley BA (2000) The effect of TiO_2 and Fe_2O_3 on metapelitic assemblages at greenschist and amphibolite facies conditions: mineral equilibria calculations in the system K_2O-FeO-MgO-Al_2O_3-SiO_2-H_2O-TiO_2-Fe_2O_3. J Metam Geol 18:497–511

White RW, Powell R, Holland TJB (2007) Progress relating to calculation of partial melting equilibria for metapelites. J Metam Geol 25:511–527

Zeh A (2001) Inference of a detailed P-T path from P-T pseudosections using metapelitic rocks of variable composition from a single outcrop, Shackleton Range, Antarctica. J Metam Geol 19:329–350

Zuluaga CA, Stowell HH, Tinkham DK (2005) The effect of zoned garnet on metapelite pseudosection topology and calculated metamorphic P-T paths. Am Mineral 90:1619–1628